HHS Public Access

Author manuscript

Nat Neurosci. Author manuscript; available in PMC 2016 October 18.

Published in final edited form as:

Nat Neurosci. 2016 June ; 19(6): 784–787. doi:10.1038/nn.4289.

Silencing spinal interneurons inhibits immune suppressive autonomic reflexes caused by spinal cord injury

Masaki Ueno[1,2], **Yuka Ueno-Nakamura**[1], **Jesse Niehaus**[1,2], **Phillip G. Popovich**[3,†], and **Yutaka Yoshida**[1,†]

[1]Division of Developmental Biology, Cincinnati Children's Hospital Medical Center, Cincinnati, Ohio, USA

[2]Precursory Research for Embryonic Science and Technology (PRESTO), Japan Science and Technology Agency (JST), Kawaguchi, Japan

[3]Center for Brain and Spinal Cord Repair, Department of Neuroscience, Wexner Medical Center, The Ohio State University Medical Center, Columbus, Ohio, USA

Abstract

Spinal cord injury (SCI) at high spinal levels (e.g., above thoracic level 5) causes systemic immune suppression; however, the underlying mechanisms are unknown. Here, we show that profound plasticity develops within spinal autonomic circuitry below the injury, creating a sympathetic anti-inflammatory reflex, and that chemogenetic silencing of this reflex circuitry blocks post-SCI immune suppression. These data provide new insights and potential therapeutic options for limiting the devastating consequences of post-traumatic autonomic hyperreflexia and post-injury immune suppression.

Spinal cord injury (SCI) above the T5 spinal level removes brain stem control over spinal autonomic circuitry causing normally innocuous stimuli below the level of injury (e.g., bladder or bowel filling) to elicit exaggerated reflex activation of sympathetic preganglionic neurons (SPNs). In SCI mice and humans, eliciting a visceral-sympathetic reflex can provoke autonomic dysreflexia (AD), a potentially fatal clinical syndrome marked by paroxysmal hypertension[1, 2]. Recently, we found that intentional and spontaneous activation of this reflex also suppresses immune function[3–5], potentially explaining why people with high-level SCI are more susceptible to infection – a leading cause of morbidity and mortality after SCI[6]. However, the neuronal substrate responsible for post-injury immune suppression has not been determined.

†Corresponding authors: Phillip G. Popovich, Phillip.Popovich@osumc.edu. Yutaka Yoshida, Yutaka.Yosida@cchmc.org.

AUTHOR CONTRIBUTIONS

P.G.P. conceived the project. P.G.P. and Y.Y. supervised the project. M.U., P.G.P. and Y.Y. designed the experiments. M.U. performed most of the experiments and analyzed data. Y.U.-N. performed surgeries and histological and flow cytometry analyses. J.N. performed histological analyses and tissue clearing. M.U., P.G.P. and Y.Y. wrote the manuscript.

T3 and T9 SCI remove or preserve, respectively, brainstem control over SPNs, and only after T3 SCI does sympathetic hyperreflexia develop with concomitant immune suppression[3, 4]. Accordingly, we first determined whether T3 and T9 SCI differentially affect the neuroanatomical substrate that connects the spinal cord with the spleen, a major secondary lymphoid organ. Consistent with previous reports[3], T3 but not T9 SCI caused profound splenic atrophy and leucopenia (Supplemental Fig. 1). To map connections between spinal cord and spleen, trans-synaptic neurotropic retrograde GFP-expressing pseudorabies virus (PRV)[7] was injected into spleens of uninjured (control) or SCI mice 28 days after a T3 or T9 SCI. In control spinal cords, PRV-GFP$^+$ cells were found ipsilateral to the intrasplenic injection (left side) within the lateral and intermediate gray matter at T4–9 spinal levels (Fig. 1a, d, g, h, m–o**; see also** Supplementary Fig. 2 and Supplementary Table 1). Such labeling is consistent with the location of the sympathetic preganglionic neurons (SPNs) previously shown to innervate rat spleen[8]. PRV-GFP$^+$ cells were found in similar numbers and distribution in control mice and T9 SCI mice (Fig. 1b, e, I, j, m–o). Conversely, although total numbers of PRV-GFP$^+$ cells within the lateral zone of the T4–T9 segment were similar after T3 SCI, they more than doubled in intermediate and medial zones of thoracic spinal cord and throughout lumbar and sacral spinal cord gray matter (Fig. 1c, f, k, l, m–o, Supplementary Fig. 3).

GFP$^+$ neurons in the medial and intermediate zones after T3 SCI are likely interneurons that form new synapses with SPNs. To distinguish SPNs from transynaptically-labeled PRV-GFP$^+$ interneurons, fluorogold (FG), a retrograde tracer, was injected into the intraperitoneal cavity (Supplementary Fig. 4a)[8, 9]. SPNs of the splenic circuit were FG/PRV-GFP-double-positive (FG$^+$/PRV$^+$), whereas interneurons do not label with FG (FG$^-$/PRV$^+$). In spinal cords from control and T9 SCI mice, FG$^+$/PRV$^+$ neurons were predominantly found in the lateral gray matter and were choline acetyltransferase-positive (CHAT$^+$) (Fig. 2a–h). Few FG$^-$/PRV$^+$ interneurons were in intermediate or medial zones (Fig. 2a–h, arrows). However, after T3 SCI, the number of FG$^-$/PRV$^+$ interneurons more than doubled in the intermediate and medial zones (Fig. 2i–l (arrows), Fig. 2m).

We next examined the phenotype of these spinal interneurons. Glutamatergic excitatory or GABAergic/glycinergic inhibitory neurons were genetically labeled using *Vglut2* (also known as *Slc17a6*)-*Cre*[10]*; CAG-lox-CAT-lox-EGFP* (*cc-EGFP*[11]) or *Vgat* (also known as *Slc32a1*)-*Cre*[10]*; cc-EGFP* mice, respectively. Most FG$^-$/PRV$^+$ interneurons were *Vglut2*-GFP$^+$ (44.0 ± 2.65% in T3 SCI; 29.2 ± 1.75% in controls) while fewer were CHAT$^+$ (18.3 ± 2.15% in T3 SCI; 47.1 ± 6.45% in controls) or *Vgat*-GFP$^+$ (9.88 ± 1.86 % in T3 SCI; 16.1 ± 0.87% in controls) (Fig. 2n–z, Supplementary Fig. 3n–q). Together, these data suggest that after T3 SCI, there is a preferential increase in connectivity between excitatory interneurons and SPNs. Consistent with this conclusion, we also observed a time-dependent increase in VGLUT2$^+$ pre-synaptic puncta contacting FG$^+$/PRV$^+$ SPNs (Supplementary Fig. 4b–h).

To determine whether enhanced structural plasticity in the spinal-splenic circuit is inherently more sensitive to activation by visceral-sympathetic reflexes, expression of c-Fos, an activity-dependent immediate early gene, was quantified after eliciting colorectal distension (CRD) in T3 SCI mice. Similar to previous reports in SCI rats[12, 13], CRD increased the number of c-Fos$^+$ neurons throughout the intermediate and medial gray matter of SCI mice

(Supplementary Fig. 5a–c). Most c-Fos$^+$ cells (>55%) were Vglut2$^+$ interneurons; <20% were CHAT$^+$ (Supplementary Fig. 5d–g).

We previously showed that both spontaneous and intentional activation of spinal autonomic reflexes cause immune suppression after T3 SCI[3]. To definitely prove a causal role for Vglut2$^+$ or CHAT$^+$ spinal interneurons in propagating immune suppressive autonomic reflexes, we silenced these neurons using chemogenetics[14]. Specifically, Gi/o-coupled human muscarinic M4 designer receptors exclusively activated by a designer drug (hM4Di DREADD) were expressed in Vglut2$^+$ or CHAT$^+$ neurons using an adeno-associated viral (AAV) vector. To target interneurons, AAV8-hSyn-DIO-hM4D(Gi)-mCherry was injected into intermediate thoracic spinal cord gray matter of *Vglut2-Cre* or *Chat-Cre* mice at P14 (Fig. 3a, Supplementary Fig. 6). Six weeks later (P56), all mice received T3 SCI and then to silence neurons, clozapine-N-oxide (CNO, 1 mg/kg)[14] was injected 2x/day from day 14–27 post-injury (Fig. 3a), when exaggerated immune suppressive reflexes develop spontaneously in SCI mice[3]. The data reveal significant silencing of hM4DGi$^+$ spinal neurons (Supplementary Fig. 7) with immune protection only in T3 SCI *Vglut2-Cre* mice injected with hM4Di DREADD and CNO. Splenic atrophy was reversed and total numbers of splenocytes, including CD4$^+$ and CD8$^+$ T cells and B220$^+$ B cells, were restored to pre-injury levels (Fig. 3b–g, Supplementary Fig. 8). Although the hM4Di DREADDs were effectively introduced into Chat$^+$ interneurons, fewer Chat$^+$ SPNs were positive for hM4Di-mCherry as compared with interneurons located in the medial or intermediate zones (medial, 38.6 ± 6.26 %; intermediate, 55.5 ± 5.17 %; lateral, 5.86 ± 1.54 %, n = 4: Supplementary Fig. 6f–i). Accordingly, only modest non-significant immune protection occurred in *Chat-Cre* mice (Fig. 3c, d).

Data in this report reveal a novel neurogenic mechanism underlying immune suppression caused by high-level SCI. Specifically, retrograde trans-synaptic labeling from the spleen reveals that a new and complex intraspinal circuitry forms after SCI, presumably due to ongoing plasticity and synaptogenesis between primary sensory afferents, interneurons and SPNs in the spinal cord. The receptive field for activating this newly formed circuit expands beyond the thoracic spinal segments that normally innervate secondary lymphoid tissues in naïve/uninjured mice. As a result, after SCI, the spontaneous activation of spinal interneurons by visceral afferents (e.g., from bladder or bowel) causes exaggerated activation of SPNs and post-ganglionic neurons that innervate vasculature, viscera and lymphoid tissues (Supplementary Fig. 9). Engaging this circuitry activates a *sympathetic anti-inflammatory reflex (SAR).* Although we have previously shown that the immune suppressive effects of SAR can be mitigated by repeat injections of adrenergic receptor antagonists[3], novel data in this manuscript show that *immune protection* can be achieved by "silencing" aberrant intraspinal circuitry. In humans, high-level SCI elicits spinal cord injury-induced immune depression syndrome (SCI-IDS), a level-dependent neurogenic mechanism of immune suppression that increases infectious complications (e.g., pneumonia)[15]. Thus, our model clinically relevant and the application of similar techniques in humans could eliminate SCI-IDS and significantly improve quality of life for those living with SCI. Since existing clinical data indicate that SCI-IDS develops without eliciting compensatory hematopoiesis[6, 16], combinatorial approaches are needed that both silence the SAR and boost hematopoiesis and subsequent immune function.

METHODS

All outcome measures were evaluated by individuals who were blind to the experimental group or individual manipulation.

Animals

C57BL/6J (Jackson laboratory), *Vglut2-Cre*[10], *Vgat-Cre*[10], *Chat-Cre*[17] and *CAG-lox-CAT-lox-EGFP* (*cc-EGFP*[11]) mice (female, 8 weeks old) were used. Mutants were backcrossed with C57/BL/6J strain at least 3 generations. Mice were maintained in a pathogen-free environment in accordance with protocols approved by the Institutional Animal Care and Use Committee of the Cincinnati Children's Hospital Medical Center. Total numbers of mice used for all studies in this report were: 116 C57BL/6J mice, 36 *Vglut2-Cre* mice (including wild-type littermate and *Vglut2-Cre; cc-EGFP* mice), 22 *Chat-Cre* mice (including wild-type littermate and *Chat-Cre; cc-EGFP* mice), and 8 *Vgat-Cre* mice (including *Vgat-Cre; cc-EGFP* mice).

PRV tracing

Bartha strain PRV152 (expressing GFP; 4.9×10^9 pfu/ml[7]) and PRV614 (expressing RFP; 3.9×10^9 pfu/ml[18]; gifts from Dr. Lynn Enquist, Princeton University) were used. Under abdominal surgery with anesthesia, PRV was injected into the spleen (10 sites, total 10 μl). Muscle and skin were then sutured. Animals were kept for indicated days and processed for histological analyses.

Spinal cord injury

Adult female mice (8 weeks of age) were anesthetized with isoflurane. A laminectomy was performed to expose the spinal cord and complete transection was performed at T3 or T9 level with iridectomy scissors and aspirator as previously described[3]. The muscle layers and skin on the back were then sutured and mice were injected with 1 ml of saline subcutaneously. They were placed in HEPA filtered cages (maximum 4 mice/cage) on the slide warmer at 37°C, under 12hr of light-dark cycle and fed commercial pellets and water *ad libitum*. Dehydration was monitored daily and manual bladder expression was conducted 2× daily. A total of 105 mice received SCI. Of these, seven mice died of unknown causes before intended date of analyses and were therefore excluded from the experiments.

Fluorogold tracing

One hundred μl of 0.4 % FG in distilled water (Fluorochrome) was injected intraperitoneally 7 days before the perfusion.

Immunohistochemistry

The animals were perfused transcardially with 4% paraformaldehyde (PFA). Spinal cords were dissected and post-fixed in the same fixatives overnight at 4°C. The tissues were then cryopreserved in 30% sucrose in PBS overnight then embedded in Tissue-Tek OCT compound (Sakura Finetek). Fifty-μm-thick serial sections (for Fig. 1a–l, Supplementary Fig. 2 and 3a–i, k–m) or 20-μm-thick of every other section (for the other experiments) were

made with a cryostat and mounted on Superfrost Plus slides (Fisher). Sections for synapse counting (Supplementary Fig. 4) were incubated in PBS overnight after fixation, embedded in low-melting agarose gel then 80-μm-thick of floating sections were made with a vibrotome (Leica).

For immunohistochemistry, sections were blocked with 1% bovine serum albumin (BSA)/ 0.3% Triton X-100 in PBS for 2 hr and then incubated with the following primary antibodies overnight at 4°C: sheep anti-GFP (1:1000; AbD Serotec, 4745-1051), rabbit anti-GFP (1:1000; Invitrogen, A11122), rat anti-GFP (1:1000; Nacalai, 04404-84), rabbit anti-RFP (Rockland, 1:1000, 600-401-379), rabbit anti-DsRed (1:500, Clontech, 632496), goat anti-choline acetyltransferase (CHAT; 1:100; Millipore, AB144P), rat anti-CD45R (B220)-FITC (1:20; BD Biosciences, 553088), rabbit anti-fluorogold (1:500, Fluorochrome), guinea pig anti-VGLUT2 (1:10000, Millipore, AB2251), and goat anti-c-Fos antibodies (1:100, Santa cruz, sc-52G). After washing with 0.1% Tween20/PBS, the sections were incubated with corresponding secondary antibodies: Alexa Fluor 488, 568, 647 or DyLight 549 donkey anti-sheep, rabbit, rat, guinea pig or goat IgG (1:1000; Invitrogen, A11015, A21206, A10042, A31573, A21208, A11055, A11057, or Jackson ImmunoResearch, 706-505-148) for 2 hr at room temperature. For labeling vibrotome sections, tissues were incubated with primary or secondary antibody 3 overnights at 4°C. Images were acquired using a wide-field fluorescence (Zeiss, AXIO IMAGER Z1) or confocal microscope (Nikon A1R$^+$).

Quantification of PRV-positive neurons

To evaluate the normal neural-splenic circuit, brains and spinal cords were analyzed at 48 (n = 2 mice), 72 (n = 2 mice), 96 (n = 2 mice), 108 (n = 1 mouse), 120 (n = 2 mice), 144 (n = 3 mice) or 168 hr (n = 2 mice) after PRV injection (Supplementary Fig. 2, Supplementary Table 1). Specific regions of the brain were identified and mapped using the atlas by Paxinos and Franklin (2001)[19]. To verify that retrograde PRV labeling from the spleen occurs via the splenic nerve and not as a result of spurious labeling due to blood-borne virus, the splenic nerve was cut before PRV injection then analyzed at 120 hr (n = 2 mice).

For counting in the spinal cord, PRV-positive cells were counted then analyzed in horizontal spinal cord sections at 96 hr after PRV injection (Fig. 1a–l, Supplementary Fig. 3). Pilot studies revealed that this time point allowed consistent labeling in SPNs and presumptive interneurons without causing overt degeneration in PRV$^+$ neurons (Supplementary Fig. 2e–g, Supplementary Table 1). Moreover, in these mice, robust labeling was evident in neuron clusters over multiple spinal segments. The total number of PRV$^+$ neurons was counted in each sub-region of the spinal cord; the left, the right, the medial zone which is along the central canal, the intermediate zone which is the central part of the gray matter, and the lateral zone which is at the interface between gray matter and white matter (see Fig. 1g). Most animals showed left side-dominant distribution (ipsilateral to PRV injection into spleen), but some animals showed an opposite tendency. Hence the quantification was done separately as ipsilateral and contralateral sides (Fig. 1m–o). The number of spinal cords analyzed were: T1–3, n = 4 mice; T4–9, n = 5 mice; T10–13, n = 4 mice; L1–5, n = 5 mice; S1–2, n = 5 mice; for each control, T9 SCI, or T3 SCI group.

Quantification of FG^+ and *Vglut2*-GFP^+, *Vgat*-GFP^+, $Chat^+$ neurons were done in horizontal sections at T4–9 spinal level. The number of spinal cords analyzed was: control, n = 4 mice; T9 SCI, n = 4 mice; T3 SCI, n = 4 mice for FG and PRV double injection experiments (Fig. 2a–m): n = 3 each for characterizing interneuron subtype (Fig. 2n–z).

In ~30% of mice (25/91), we observed no labeling or very few PRV^+ cells (~10 cells in the lateral edge of the gray matter) in the thoracic cord. This variability was not specific to any experimental group and was considered an intrinsic variability in injection and/or uptake of the virus. Samples from these mice were excluded from further analyses.

Quantification of Vglut2$^+$ presynaptic puncta on SPNs

Horizontal floating sections (T4–9 level) were stained with rabbit anti-FG, sheep anti-GFP, and guinea pig anti-vGlut2 antibodies (80-μm-thick) then were mounted on slides and coverslipped. Z-stack images were acquired with confocal microscopy. FG^+/PRV-GFP^+ SPNs with their entire cell body localized within the plane of section and not overlapped with other cells were selected and 3D images were reconstructed using Imaris software (BITPLANE). $VGlut2^+$ puncta on the surface of GFP^+ SPN soma were manually selected and the density ($Vglut2^+$ puncta number/GFP^+ surface) was calculated. The number of animals analyzed were: controls without injury, n = 2 mice (44 cells); day 7 after T3 SCI, n = 3 mice (29 cells); day 10, n = 1 mouse (10 cells); day 28, n = 5 mice (67 cells). Data of day 7 and 10 were pooled into one group as a time interval that precedes post-SCI immune suppression[3].

PACT clearing of spleen

Spleens were cleared using the passive CLARITY (PACT) protocol[20]. Harvested spleens were fixed in 4% PFA overnight and washed in PBS. The samples were incubated overnight at 4°C in A4P0 hydrogel monomer solution (4% acrylamide and 0% PFA in PBS), containing 0.25% photoinitiator 2,2′-Azobis[2-(imidazolin-2-yl)propane] dihydrochloride (VA-044, Wako). To polymerize the tissue-hydrogel matrix, samples were then incubated in a 37°C oven with shaker for 2–3 hr. Polymerized tissues were washed with PBS and then transferred to a clearing solution containing 8% SDS diluted in 0.1M PBS and incubated at 37°C for 5 days with shaking. The samples were washed with 5 changes of PBS over 1 day and were incubated in blocking solution containing 10% normal donkey serum, 0.1% triton X-100 and 0.01% sodium azide at room temperature for 24 hr with shaking. They were then incubated with rabbit anti-tyrosine hydroxylase (TH) antibody (1:500, Millipore, AB152) in blocking solution at 4^0 C for 4 days. They were washed with 5 changes of PBS over 1 day and incubated with Alexa 568 donkey anti-rabbit IgG antibody (1:500, Invitrogen) in blocking solution at 4^0 C for 2 days. They were washed with 5 changes of PBS over 1 day and incubated in RIMS solution (88% Histodenz, 0.01% Sodium azide in 0.02M phosphate buffer, pH to 7.5) for 24 hr. Images were acquired using a multiphoton confocal microscope (Nikon, A1MP).

Colorectal distension (CRD) and c-Fos analyses

Colorectal distension was induced as previously reported[3, 12, 13] with minor modification. A 4-French, 60 mm balloon-tipped catheter (Swan-Ganz monitoring catheter model 116F4;

Edwards Life Sciences) was inserted 1.5 cm into the rectum before securing the catheter to the tail with surgical tape. The balloon was inflated with 0.2 ml of air for 30 sec then deflated 60 sec. This 90 sec cycle was repeated for 90 min. Mice were perfused 30 min after the final cycle of inflation. The number of c-Fos$^+$ cells were counted and analyzed in 2 representative horizontal spinal cord sections at T4–9 level from multiple SCI animals with or without CRD stimulation. The number of animals analyzed were: uninjured with or without CRD, n = 3 mice/group; T3 SCI (day 28) without CRD, n = 3 mice; T3 SCI (day 28) with CRD, n = 5 mice; *Vglut2-Cre; cc-EGFP* + T3 SCI (day 28) with CRD, n = 3 mice; *Chat-Cre; cc-EGFP* + T3 SCI (day 28) with CRD, n = 3 mice (Supplementary Fig. 5). To evaluate the effects of DREADD in mice with CRD-induced activation of visceral-sympathetic reflex, CNO (1.0 mg/kg body weight, i.p.; Sigma) or vehicle saline was injected into *Vglut2-Cre* + T3SCI + AAV8-hSyn-DIO-hM4D(Gi)-mCherry mice at day 28 post-injury, 30 min before the induction of CRD (n = 3 mice each) (Supplementary Fig. 7).

DREADD experiment

AAV8-hSyn-DIO-hM4Di-mCherry (AAV8-hSyn-DIO-hM4D(Gi)-mCherry; 7×10^{12} vg/ml; UNC Vector Core) was injected into T5 and 7 levels of the spinal cord of *Vglut2-Cre*, *Chat-Cre*, or WT mice at P14 (0.8 μl/site, 0.25 mm lateral, 0.5 mm in depth). We confirmed that AAV-mediated transduction was restricted to neurons within and adjacent to the injection site and virus did not get retrogradely transported into brain stem (Supplementary Fig. 6k). T3 SCI was induced at 8 weeks old, and then CNO (1.0 mg/kg body weight, i.p.; Sigma) was injected twice per day from day 14 to 27 post-injury (Fig. 3a). Small cohorts of mice from each colony were randomly chosen for each experimental group and used as they reached the appropriate age for experimentation. Total number of mice used across different experiments were: WT control, 3 separate rounds (n = 3, 3, 3, total n = 9 mice); WT + T3 SCI, 5 separate rounds (n = 2, 1, 2, 2, 1, total 8 mice); WT + T3 SCI + AAV8-hSyn-DIO-hM4Di-mCherry +CNO, 3 rounds (n = 4, 2, 2, total 8 mice); *Vglut2-Cre* + T3 SCI + AAV8-hSyn-DIO-hM4Di-mCherry + CNO, 5 rounds (n = 2, 1, 1, 2, 2, total 8 mice); *Chat-Cre* + T3 SCI + AAV8-hSyn-DIO-hM4Di-mCherry +CNO, 4 rounds (n = 4, 1, 1, 2, total 8 mice). In some experiments, spleens were fixed via immersion in 4% PFA fixation (i.e, no flow cytometry analyses; WT control, n = 4 mice; WT + T3 SCI, n = 5 mice; WT + T3 SCI + AAV8-hSyn-DIO-hM4Di-mCherry + CNO, n = 4 mice; *Vglut2-Cre* + T3 SCI + AAV8-hSyn-DIO-hM4Di-mCherry + CNO, n = 4 mice; *Chat-Cre* + T3 SCI + AAV8-hSyn-DIO-hM4Di-mCherry +CNO, n = 6 mice). Female C57BL/6J mice were used for WT control and WT + T3 SCI group, and WT littermate with *Vglut2-Cre* and *Chat-Cre* mice (n = 4 mice, each) were used for WT + T3 SCI + AAV8-hSyn-DIO-hM4Di-mCherry + CNO group.

Flow cytometry

Spleens were harvested in Flow Cytometry Staining Buffer (eBioscience) and cell suspensions were made by expressing spleen tissue through a cell strainer using the plunger of a 10 ml syringe. Cell suspensions were then washed, centrifuged and resuspended in 1 ml of the buffer. Splenocytes were counted on a hemocytometer and 5×10^5 cells were incubated with Fc-block (anti-mouse-CD16/CD32 antibody; eBioscience). Samples were stained with the following antibodies: anti-CD45R (B220)-FITC (clone RA3-6B2; BD Biosciences), anti-CD4-FITC (clone GK1.5; BD Biosciences), anti-CD8-PE (clone 53-6.7;

BD Biosciences), and isotype-specific control anti-rat IgG2a κ-FITC and -PE antibodies (clone R35-95; BD Biosciences). All antibodies were diluted to 0.5 μg for 5×10^5 cells. Splenocytes (10,000 events/sample) were analyzed using a FACSCanto flow cytometer with FACSDiva software (BD Biosciences). Data analyses were conducted with FlowJo software (FlowJo). Dot plots of forward scatter (FSC) vs side scatter (SSC) were used to exclude debris, and then doublets were excluded using FSC-height (H) vs FSC-width (W) and SSC-H vs SSC-W plots (Supplementary Fig. 8). The number of each subset was calculated as the percentage of labeled cells multiplied by the total number of splenocytes.

Statistical analyses

Quantitative data are expressed as the mean ± s.e.m. No statistical methods were used to predetermine sample sizes, but our sample sizes are comparable to those reported in previous publications[3,8]. Statistical analyses were performed using Prism 6 (GraphPad). Differences among the groups were analyzed by one-way ANOVA followed by Tukey test or Kruskal-Wallis test followed by Dunn's multiple comparisons test. Normality and equality of variances among the groups were analyzed with D'Agostino-Pearson normality test and Brown-Forsythe test, respectively. Differences between experimental group pairs were analyzed with Student's *t* test (two tailed). Normality and equality of variances between the groups were analyzed with D'Agostino-Pearson normality test and F test, respectively. When the sample numbers were too small to calculate, distribution was assumed to be normal. A *P*-value less than 0.05 was considered significant.

Supplementary Material

Refer to Web version on PubMed Central for supplementary material.

Acknowledgments

We would like to thank L. Enquist (Princeton University) for providing PRV; Y. Zhang (The Ohio State University) for advising on SCI surgery; Z. Gu and S. Goyama for helpful comments, P. Thanh, A. Epstein, M. Sandy, and M. Maezawa for helping experiments, and M. Muntifering for clearing technique (Cincinnati Children's Hospital). This work is supported by NINDS-NS083942 and the Ray W. Poppleton Endowment (P.G.P.); NINDS-NS093002 (Y.Y.); PRESTO (JST), JSPS Postdoctoral Fellowships for Research Abroad and KANAE Foundation for the Promotion of Medical Science (M.U.).

References

1. Blackmer J. Rehabilitation medicine: 1. Autonomic dysreflexia. CMAJ. 2003; 169:931–935. [PubMed: 14581313]
2. Inskip JA, Ramer LM, Ramer MS, Krassioukov AV. Autonomic assessment of animals with spinal cord injury: tools, techniques and translation. Spinal Cord. 2009; 47:2–35. [PubMed: 18542091]
3. Zhang Y, et al. Autonomic dysreflexia causes chronic immune suppression after spinal cord injury. J Neurosci. 2013; 33:12970–12981. [PubMed: 23926252]
4. Lucin KM, Sanders VM, Jones TB, Malarkey WB, Popovich PG. Impaired antibody synthesis after spinal cord injury is level dependent and is due to sympathetic nervous system dysregulation. Exp Neurol. 2007; 207:75–84. [PubMed: 17597612]
5. Lucin KM, Sanders VM, Popovich PG. Stress hormones collaborate to induce lymphocyte apoptosis after high level spinal cord injury. J Neurochem. 2009; 110:1409–1421. [PubMed: 19545280]
6. Meisel C, Schwab JM, Prass K, Meisel A, Dirnagl U. Central nervous system injury-induced immune deficiency syndrome. Nat Rev Neurosci. 2005; 6:775–786. [PubMed: 16163382]

7. Smith BN, et al. Pseudorabies virus expressing enhanced green fluorescent protein: A tool for in vitro electrophysiological analysis of transsynaptically labeled neurons in identified central nervous system circuits. Proc Natl Acad Sci U S A. 2000; 97:9264–9269. [PubMed: 10922076]
8. Cano G, Sved AF, Rinaman L, Rabin BS, Card JP. Characterization of the central nervous system innervation of the rat spleen using viral transneuronal tracing. J Comp Neurol. 2001; 439:1–18. [PubMed: 11579378]
9. Anderson CR, Edwards SL. Intraperitoneal injections of Fluorogold reliably labels all sympathetic preganglionic neurons in the rat. J Neurosci Methods. 1994; 53:137–141. [PubMed: 7823616]
10. Vong L, et al. Leptin action on GABAergic neurons prevents obesity and reduces inhibitory tone to POMC neurons. Neuron. 2011; 71:142–154. [PubMed: 21745644]
11. Nakamura T, Colbert MC, Robbins J. Neural crest cells retain multipotential characteristics in the developing valves and label the cardiac conduction system. Circ Res. 2006; 98:1547–1554. [PubMed: 16709902]
12. Hou S, et al. Plasticity of lumbosacral propriospinal neurons is associated with the development of autonomic dysreflexia after thoracic spinal cord transection. J Comp Neurol. 2008; 509:382–399. [PubMed: 18512692]
13. Duale H, Lyttle TS, Smith BN, Rabchevsky AG. Noxious colorectal distention in spinalized rats reduces pseudorabies virus labeling of sympathetic neurons. J Neurotrauma. 2010; 27:1369–1378. [PubMed: 20528165]
14. Sternson SM, Roth BL. Chemogenetic tools to interrogate brain functions. Annu Rev Neurosci. 2014; 37:387–407. [PubMed: 25002280]
15. Brommer B, et al. Spinal cord injury-induced immune deficiency syndrome enhances infection susceptibility dependent on lesion level. Brain. 2016
16. Iversen PO, et al. Depressed immunity and impaired proliferation of hematopoietic progenitor cells in patients with complete spinal cord injury. Blood. 2000; 96:2081–2083. [PubMed: 10979951]
17. Rossi J, et al. Melanocortin-4 receptors expressed by cholinergic neurons regulate energy balance and glucose homeostasis. Cell Metab. 2011; 13:195–204. [PubMed: 21284986]
18. Banfield BW, Kaufman JD, Randall JA, Pickard GE. Development of pseudorabies virus strains expressing red fluorescent proteins: new tools for multisynaptic labeling applications. J Virol. 2003; 77:10106–10112. [PubMed: 12941921]
19. Paxinos, G. The mouse brain in stereotaxic coordinates. Academic press; San Diego, CA: 2001.
20. Yang B, et al. Single-cell phenotyping within transparent intact tissue through whole-body clearing. Cell. 2014; 158:945–958. [PubMed: 25088144]

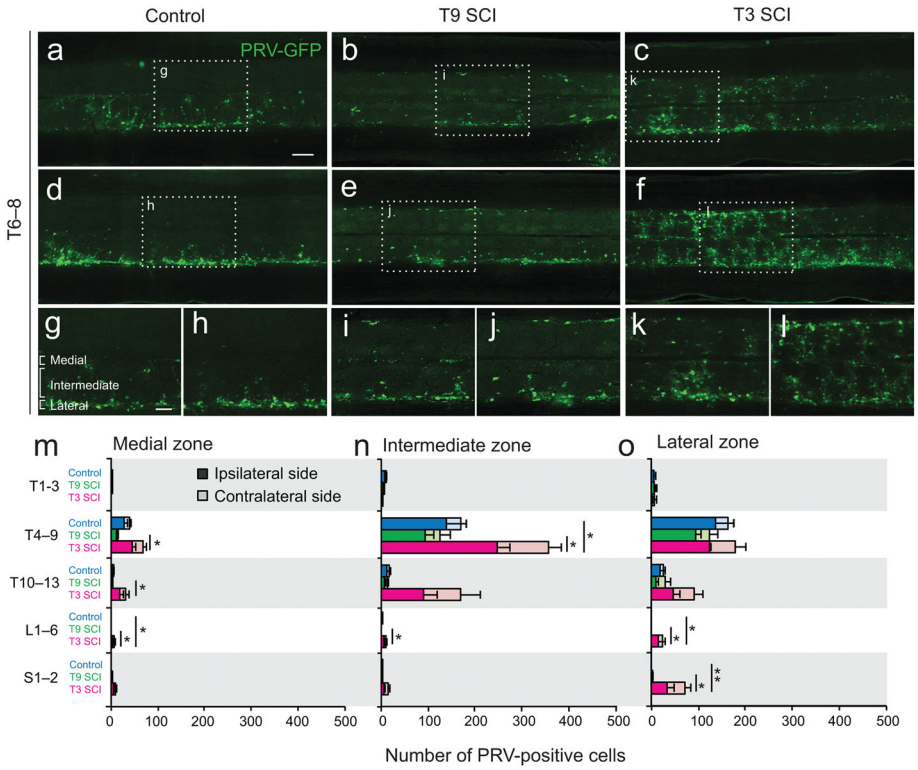

Figure 1.

Trans-synaptic labeling of spinal cord-spleen circuit in T3 SCI mice. (**a–l**) Horizontal sections of spinal cord in control (**a**, **d**, **g**, **h**), T9 SCI (**b**, **e**, **i**, **j**), and T3 SCI mice (**c**, **f**, **k**, **l**), 96 hr after intrasplenic PRV injection. Images of 2 serial adjacent sections of T6–8 are shown, stained with anti-GFP antibody (green). Rostral is left. Magnified view of dotted squares in **a**–**f** are shown in **g**–**l**, respectively. Scale bars, 200 μm (**a**–**f**); 100 μm (**g**–**l**). The images are representative of 4 independent experiments. (**m**–**o**). Number of PRV-positive cells was quantified in medial (**m**), intermediate (**n**), and lateral zone (**o**) of the spinal cord gray matter (see **g**) from T1 to S2 level then were compared between control (blue bars), T9 SCI (green bars), and T3 SCI mice (magenta bars). Dark bars, ipsilateral side; light bars, contralateral side of the spinal cord. Data are represented as mean ± s.e.m (n = 4 mice for T1–3 and T10–13, n = 5 mice for others). One way ANOVA followed by Tukey test or Kruskal-Wallis test followed by Dunn's multiple comparisons test; $p = 0.0121$, 0.0151, 0.0194, 0.0194 (**m**, up to bottom), $p = 0.0414$, 0.033. 0.0279 (**n**), $p = 0.0194$, 0.0194, 0.0043, 0.0157 (**o**); $*p < 0.05$, $**p < 0.01$.

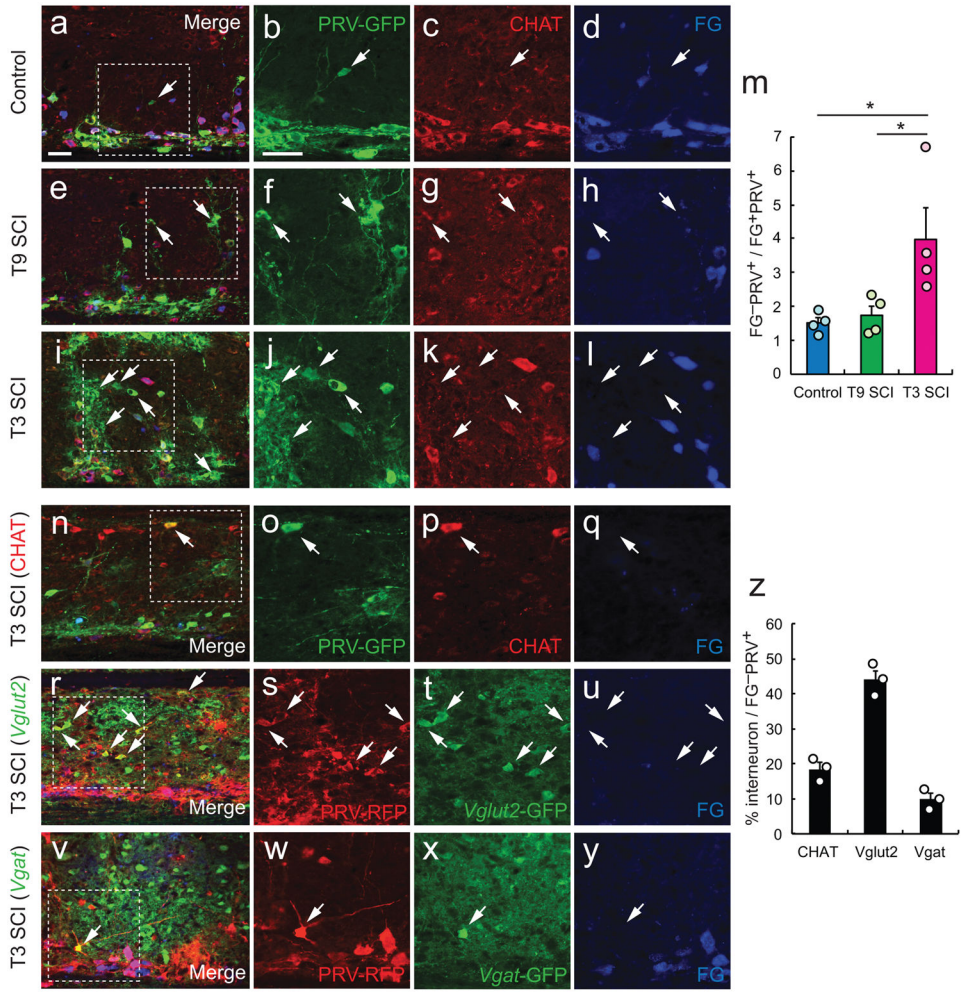

Figure 2.

Identification of spinal interneurons in the spinal cord-splenic sympathetic circuit. (**a**–**l**) GFP (PRV, green), Chat (red), and FG (blue) labeled neurons at T6 spinal level in control (**a**–**d**), T9 SCI (**e**–**h**), and T3 SCI mice (**i**–**l**) after double-labeling with FG (i.p.) and PRV (intrasplenic). Horizontal spinal cord sections are oriented with rostral edge of spinal cord to the left. Dotted boxes in left panels are magnified in individual channels to the right. Arrows indicate FG^-/PRV^+ spinal interneurons. Scale bars, 50 μm (**a** for left panels, **b** for others). Images are representative of 4 independent experiments. (**m)** Quantification of the ratio of spinal interneurons (FG^-/PRV^+) to SPNs (FG^+/PRV^+). Data are represented as mean ± s.e.m (n = 4 mice). One way ANOVA followed by Tukey test; $p = 0.0315, 0.0487$ (left to right); $*p < 0.05$. (**n**–**y**) Neurotransmitter subtype of spinal interneurons in T3 SCI. (**n**–**q**) GFP (PRV, green), Chat (red), and FG (blue). (**r**–**u**) RFP (PRV, red), GFP (*Vglut2*, green), and FG (blue) in *Vglut2-Cre; cc-EGFP* mice. (**vy**) RFP (PRV, red), GFP (*Vgat*, green), and FG (blue) in *Vgat-Cre; cc-EGFP* mice. Arrows indicate double-positive interneurons (FG^-). Images are representative of 3 independent experiments. (**z**) The ratio of $Chat^+$, *Vglut2*-GFP^+ and *Vgat*-GFP^+ in FG^-/PRV^+ spinal interneurons in T3 SCI mice (n = 3 mice).

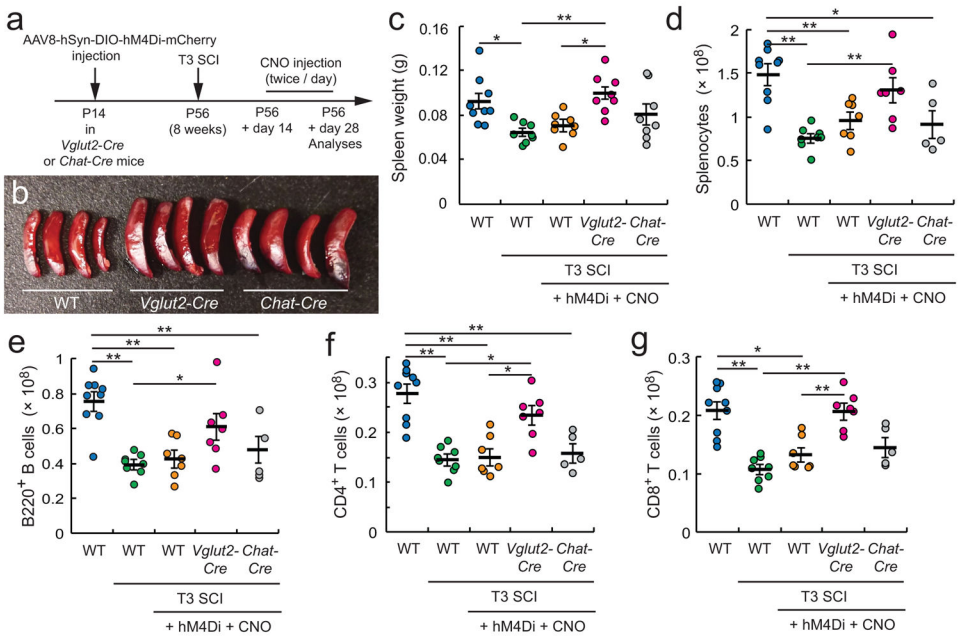

Figure 3.

Chemogenetic silencing of spinal interneurons rescues immune cells after T3 SCI. (**a**) Experimental time course. (**b**) Image of spleens from individual mice at day 28 after T3 SCI of wild-type, *Vglut2-Cre* and *Chat-Cre* mice injected with AAV-hSyn-DIO-hM4Di-mCherry and CNO (+ hM4Di + CNO). (**c**) Wet spleen weights at day 28 post-injury. Thick horizontal bars represent the mean values and error bars are s.e.m. WT control, n = 9 mice; other groups, n = 8 mice. (**d**) The number of total splenocytes. (**e**–**g**) The number of $B220^+$ B cells (**e**), $CD4^+$ (**f**) and $CD8^+$ T cells (**g**). WT control, n = 9 mice; WT + T3 SCI, n = 8 mice; WT + hM4Di + T3 SCI + CNO, n = 7 mice; *Vglut2-Cre* + hM4Di + T3 SCI + CNO, n = 7 mice; *Chat-Cre* + hM4Di + T3 SCI + CNO, n = 5 mice; One way ANOVA followed by Tukey test; p = 0.0409, 0.0037, 0.0248 (**c**, left to right), p = 0.0001, 0.0084, 0.0103, 0.0094 (**d**), p = < 0.0001, 0.0005, 0.0035, 0.0422 (**e**), p = < 0.0001, 0.0002, 0.0018, 0.0106, 0.0263 (**f**), p = 0.0001, 0.0152, 0.0002, 0.0097 (**g**); *p < 0.05, **p < 0.01.